Minimizing Performance Degradation Induced by Interfacial Recombination in Perovskite Solar Cells through Tailoring of the Transport Layer Electronic Properties

UT Dallas Author(s):

Liang Xu
Rouzbeh Molaei Imenabadi
William G. Vandenberghe
Julia W. P. Hsu

Citation:

Xu, Liang, Rouzbeh Molaei Imenabadi, William G. Vandenberghe, and Julia W. P. Hsu. 2018. "Minimizing performance degradation induced by interfacial recombination in perovskite solar cells through tailoring of the transport layer electronic properties." APL Materials 6(3): Art. 036104, doi:10.1063/1.5021138

Minimizing performance degradation induced by interfacial recombination in perovskite solar cells through tailoring of the transport layer electronic properties

Liang Xu, Rouzbeh Molaei Imenabadi, William G. Vandenberghe,[a] and Julia W. P. Hsu[a]
Department of Materials Science and Engineering, University of Texas at Dallas, Richardson, Texas 75080, USA

(Received 1 January 2018; accepted 28 February 2018; published online 20 March 2018)

The performance of hybrid organic-inorganic metal halide perovskite solar cells is investigated using one-dimensional drift-diffusion device simulations. We study the effects of interfacial defect density, doping concentration, and electronic level positions of the charge transport layer (CTL). Choosing CTLs with a favorable band alignment, rather than passivating CTL-perovskite interfacial defects, is shown to be beneficial for maintaining high power-conversion efficiency, due to reduced minority carrier density arising from a favorable local electric field profile. Insights from this study provide theoretical guidance on practical selection of CTL materials for achieving high-performance perovskite solar cells. https://doi.org/10.1063/1.5021138

Hybrid organic-inorganic metal halide perovskite solar cells (PSCs) have experienced tremendous performance boosts within the past decade. With a state-of-the-art power conversion efficiency (PCE) beyond 22% already,[1] the PSCs promisingly rival other established photovoltaic material systems with much lower fabrication cost. A large absorption coefficient, a high charge carrier mobility, long diffusion lengths, and a low exciton binding energy associated with the hybrid perovskite materials[2,3] are responsible for the excellent photovoltaic performance in PSCs. In particular, the intrinsically low non-radiative bulk recombination rates in the perovskite materials uphold the promise for PSC performance to reach its theoretical limit.[4–6] With these superior properties of the perovskite active materials, the next phase of increasing PSC performance will require understanding and optimization of other parts of PSCs, specifically the charge transport layers (CTLs) to minimize interfacial recombination—a major loss mechanism.[7–9]

To this date, CTL research has focused on mobility/conductivity,[10] film morphology,[11] interfacial defect passivation,[12,13] photocurrent hysteresis,[14] device stability,[15] as well as electronic structure.[12,16–18] Especially, the CTL electronic structure has always been in the research spotlight: while it has been reported to affect the device performance,[12,16] other work observes less detrimental effects due to the potential interfacial dipoles from ionic accumulation near the interface.[17] Moreover, it was suggested that the interfacial defects play a more important role than the energy level positions in determining the device photovoltaic performance.[18] While fundamental understandings on the importance of CTL electronic structure is crucial to further boost PSC performance, experimentally it is hard to distinguish the separate contribution from electronic structure, interfacial defects, or possible surface dipoles. In contrast, device simulation provides the full capability of examining the impact from each contribution as well as different combinations. A previous simulation study by Minemoto and Murata[19] has shed some light on this topic, but since they used a 10-nm artificial defect layer with a reduced bandgap to model recombination at the CTL-perovskite interface, band alignment becomes unrealistic, ultimately limiting the robustness of the results. Moreover, insights from the

[a]Authors to whom correspondence should be addressed: william.vandenberghe@utdallas.edu and jwhsu@utdallas.edu.

underlying physical mechanisms, beyond the basic current density-voltage (J-V) results, are highly beneficial to understand and guide experiments.

In this paper, based on a one-dimensional (1D) drift-diffusion simulation study, we demonstrate that CTLs with favorable electronic level positioning and band alignment effectively reduce the detrimental effect of interfacial recombination in the presence of defects at the CTL-perovskite interfaces and therefore preserve high PCE in the PSCs. This "cliff and spike effect" is widely reported in inorganic heterojunction solar cells, e.g., copper-indium-gallium-selenide solar cells.[20] By taking the hole transport layer (HTL) as an example, we show that, at a forward bias approaching the open-circuit voltage (V_{oc}), a HTL with deep energy levels, i.e., a large electron affinity or a high dopant density, exhibits stronger band bending and thus a larger electrical field at the perovskite-HTL heterojunction interface. This field drives minority carriers (electrons) in the perovskite layer away from the HTL interface and effectively reduces recombination through the interfacial defects, which inevitably exist.[5] Thus, deep energy level HTLs exhibit only a slight performance reduction even with a relatively high interfacial defect density. On the other hand, device performance, particularly V_{oc} and fill factor (FF), reduces dramatically even at a very low interface defect density when the HTL energy levels are shallow. The same principle applies to electron transport layers (ETL), in which shallow energy levels reduce the impact of interfacial recombination. Recently, HTLs with deep energy levels, including $CuGaO_2$,[21] $CuCrO_2$,[22] and NiO_x,[23] as well as shallow energy level ETLs, such as $SrTiO_3$,[24] have been demonstrated to achieve high-performance PSCs. Since a defect-free heterojunction interface is unlikely in real devices and interfacial defect passivation usually requires tremendous research efforts and varies case by case,[12,13] this study provides a useful guideline for a more practical and robust approach to the CTL design and performance boost in PSCs.

The device simulations are carried out with the commercial semiconductor simulation tool Sentaurus Device from Synopsys.[25] A *p-i-n* structured perovskite solar cell is modeled with planar junctions[26–28] consisting of a transparent conducting oxide anode, a *p*-type semiconductor HTL (30 nm), a methylammonium lead iodide perovskite layer (400 nm), a phenyl-C61-butyric acid methyl ester (PCBM) ETL (*n*-type, 20 nm), and an Al cathode. Table S1 of the supplementary material summarizes input parameters for each layer. Particularly, the experimentally measured energy levels of a *p*-type delafossite oxide $CuCrO_2$,[29] which has been demonstrated to be a promising HTL candidate for PSCs,[22] are adopted as the starting point in the simulations, with a variation in energy level positions discussed in Fig. 1. While this work only studies the impact of HTL energy levels in detail, the results are readily applied to ETLs (Fig. S1 of the supplementary material).

Shown in Fig. 1, we vary the HTL energy levels in two ways: (1) varying the electron affinity (EA or conduction band minimum) while keeping the bandgap (E_g) of the HTL constant [Fig. 1(a)] and (2) varying the Fermi level (E_f) by varying the doping concentration (N_A) of the HTL but keeping the EA and E_g unchanged [Fig. 1(b)]. Note that when the EA is changed in (1), E_f will also change since the doping is kept constant. Interfacial recombination is modeled by a neutral-type single level defect located at mid-gap, where the trap-assisted recombination is most effective.[30,31] Simulations using a shallow defect level that matches experimentally obtained values for bulk defects in the perovksite layer[32] are also performed (Fig. S2 of the supplementary material), which show similar

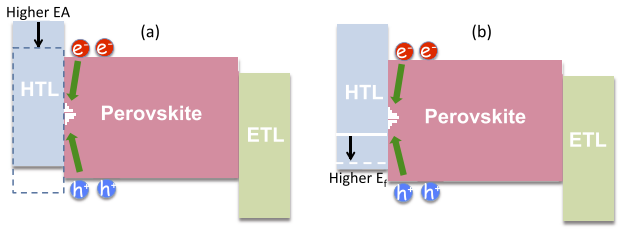

FIG. 1. Schematic of the device structure used in our simulations. The HTL electronic level position is varied through (a) varying the HTL EA while keeping E_g unchanged and (b) varying the HTL E_f through dopant concentration (N_A). Green arrows indicate the interfacial recombination of electrons and holes through the defect states at the HTL-perovskite interface (short line at the interface).

behavior compared to the mid-gap defect scenario; hence, the rest of the paper is based on the mid-gap recombination center. With the presence of defect states at the HTL-perovskite interface, the electrons (minority carriers at this interface) recombine with the holes (majority carriers), resulting in the interfacial recombination loss (as the green arrows indicate).

The device PCEs that are computed as the maximum power output (product of voltage and current) normalized to incident illumination power, with varying EA and N_A (E_f), are shown in Figs. 2(a) and 2(b), respectively. We first consider the scenario of the HTL-perovskite interface without defects [red symbols in Figs. 2(a) and 2(b)]. Negligible PCE changes are observed by varying either EA or N_A, implying that the HTL electronic level position by itself has little impact on the PSCs. However, when introducing interfacial defects at a density (N_t) of 1×10^{11} cm^{-2},[30,31] a definitive trend is observed as a function of EA or N_A [black symbols in Figs. 2(a) and 2(b)]: a significant reduction in PCE is seen in both lower EA and N_A devices; as EA or N_A increases, the PCE recovers its defect-free value. With N_A fixed at 3.8×10^{18} cm^{-3}, the PCE improvement starts to saturate at an EA of 2.4 eV, where the valence band maximum (VBM) of HTL is 0.1 eV deeper than that of perovskite [$\Delta E_{VB} = 0.1$ eV as shown in the top x-axis of Fig. 2(a)]. On the other hand, given a fixed EA of 2.3 eV, a full recovery of the PCE is observed when N_A increases to 3.8×10^{20} cm^{-3}, which results in a HTL Fermi level 0.19 eV deeper than the VBM of the perovskite [$E_{f,HTL} - E_{VB,perovskite} = 0.19$ eV as shown in the top x-axis of Fig. 2(b)]. To understand this behavior, J-V characteristics are shown in Figs. 2(c) and 2(d) for high (green symbols) and low (blue symbols) EA and N_A values, respectively. Significant reductions of the collected current density (J_{coll}, solid symbols) are observed at all bias conditions in the low EA and N_A value devices; the current loss is due

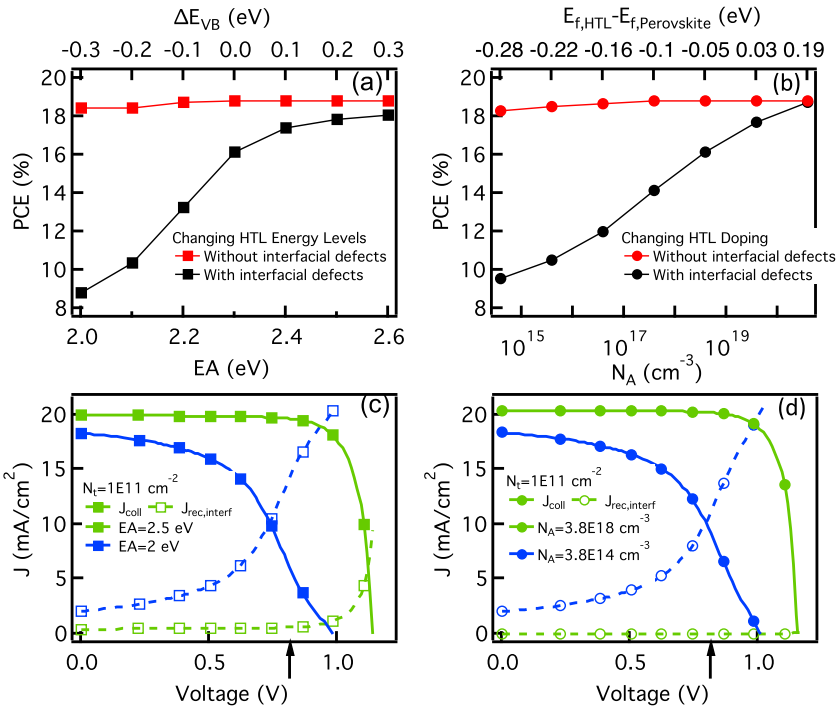

FIG. 2. (a) Simulated PCEs for devices with varying EA without (red squares) and with (black squares) interfacial defects. The corresponding energy difference between the VBM of the HTL and that of the perovskite (ΔE_{VB}) is shown on the top x-axis. N_A is fixed at 3.8×10^{18} cm^{-3}. (b) Simulated PCEs for devices with varying N_A without (red circles) and with (black circles) interfacial defects. The corresponding energy difference between the Fermi level of the HTL and the VBM of the perovskite ($E_{f,HTL} - E_{VB,perovskite}$) is shown on the top x-axis. The EA is fixed at 2.3 eV. (c) Collected current density (J_{coll}) and interfacial recombination current ($J_{rec,interf}$) vs. voltage for devices with an HTL EA of 2.5 eV (green) and 2 eV (blue). (d) J_{coll} and $J_{rec,interf}$ vs. voltage for devices with a HTL N_A of 3.8×10^{18} cm^{-3} (green) and 3.8×10^{14} cm^{-3} (blue). In (c) and (d), the devices all have interfacial defects with a N_t of 1×10^{11} cm^{-2}, and solid lines with solid symbols represent J_{coll}, while dashed lines with open symbols represent $J_{rec,interf}$. The arrows indicate the bias of 0.8 V, which is discussed later. All results are simulated under 1 Sun illumination.

to the enhanced interfacial recombination current density ($J_{rec,interf}$, open symbols). This is particularly evident as the bias approaches its maximum power point, resulting in a significant degradation in FF. In contrast, devices with a higher EA or N_A HTL retain a high J_{coll} and a low $J_{rec,interf}$ all the way up to V_{oc}. In other words, a HTL with deeper energy levels is less susceptible to recombination at the HTL-perovskite interface.

To further elucidate the observed effects of the HTL electronic level position on device performance, we closely examine the electric field, the band diagram, as well as the charge distribution in the devices. We only discuss the case of varying EA values in Figs. 3 and 4 since similar results are found for varying N_A values (shown in Figs. S3 and S4 of the supplementary material). We perform our investigation at a bias of 0.8 V [indicated by the arrow in Figs. 2(c) and 2(d)], where J_{coll} and $J_{rec,interf}$ show a dramatic difference between the high and low EA devices. The interfacial defect density is the same, $N_t = 1 \times 10^{11}$ cm^{-2}, for all cases. As illustrated in Fig. 3(a), under illumination, a significantly larger electrical field near the HTL-perovskite interface (indicated by the arrow) is seen in the device with the higher EA HTL (green). (The electrical field profile and band alignment are independent of interfacial defects because HTL Fermi levels are not pinned to the interfacial defect states.) This marked difference in electric field comes from the local band alignment as shown in the inset of Fig. 3(a). (Figure 3 only shows the region near the HTL-perovskite interface. The band diagrams and electron density distributions across the entire device are shown in Fig. S5 of the supplementary material.) Stronger band bending appears across the HTL-perovskite interface in the device with the higher EA HTL, even at a relatively large forward bias of 0.8 V. The correspondingly larger local electrical field in the light-absorbing perovskite layer effectively drives the photo-generated minority carriers (electrons) away from the interface. Without such a local electrical field, a significant number of minority carriers reach the interface through diffusion. As shown in Fig. 3(b), by comparing the two "ideal" devices without interfacial defects (dashed lines), the device with a HTL EA of 2 eV has an electron density in the perovskite layer near the interface 2 orders of magnitude larger compared to the device with a HTL EA of 2.5 eV (the electron density drops abruptly at the interface because of it being extremely low in the HTL). In the presence of defects (solid lines), i.e., recombination centers, these electrons readily recombine with holes at the HTL-perovskite interface, resulting in a higher recombination rate at the interface. With a larger EA HTL, the electron densities at the interface are similarly low with and without defects [Fig. 2(d) green lines]. Effectively, the HTL with the higher EA reduces the interfacial recombination by preventing the minority carriers from reaching the defect states/recombination centers at the HTL-perovskite interface. A similar interfacial recombination reduction effect is also observed in the devices with a more highly doped HTL (Fig. S3 of the supplementary material).

We further examine the dependence on interfacial defect density N_t for HTLs with various EA values in Fig. 4. All values are normalized to the case without interfacial defects to better illustrate

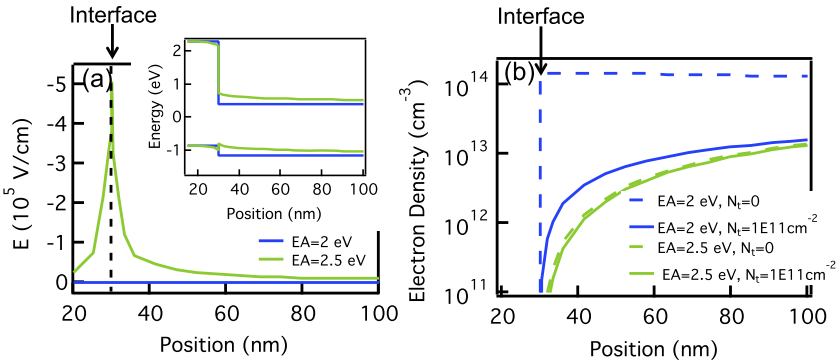

FIG. 3. (a) Electrical field vs. position near the HTL-perovskite interface under 1 Sun illumination for the devices with a HTL EA of 2 eV (blue) and 2.5 eV (green). The black dashed line indicates the interface position. The inset shows the band diagram near the interface. (b) Electron density vs. position for the device; dashed lines denote the cases without defects at the CTL-perovskite interface and solid lines denote the cases with interfacial defects at a density $N_t = 1 \times 10^{11}$ cm^{-2}. The color scheme is the same as that in Fig. 2(c).

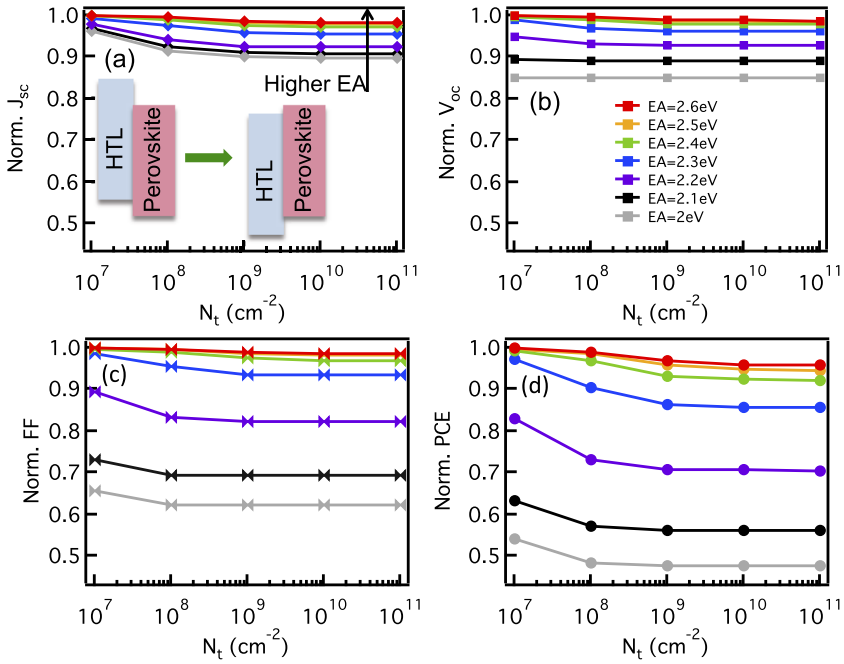

FIG. 4. Simulated J_{sc} (a), V_{oc} (b), FF (c), and PCE (d) for devices with different EA values for the HTL: 2.6 eV (red), 2.5 eV (orange), 2.4 eV (green), 2.3 eV (blue), 2.2 eV (purple), 2.1 eV (black), and 2 eV (gray). The arrow indicates the direction of increasing EA, as depicted in the inset of (a) for the two extreme cases. All parameters are normalized to the values of devices without interfacial defects.

the effects of increasing interface defect concentration on device performance (see Fig. S6 of the supplementary material for parameters without normalization). While J_{sc} [Fig. 4(a)] decreases moderately with increasing N_t for all EA values, the reduction is less significant for the case of higher HTL EA. In the device with a HTL EA of 2.6 eV (the VBM of the HTL is 0.3 eV larger than that of the perovskite layer), a marginal reduction (~2%) is observed at the highest simulated defect density N_t of 10^{11} cm^{-2}, indicating that J_{sc} loss due to interfacial recombination is minimal. Similarly, V_{oc} and FF demonstrate negligible reductions at N_t of 10^{11} cm^{-2} with the HTL EA of 2.6 eV. However, much more significant decreases in both V_{oc} and FF are seen at lower interface defect densities for lower EA values [Figs. 4(b) and 4(c)]. In other words, V_{oc} and FF are less dependent on N_t but more dependent on the HTL energy levels. Because J_{sc} is determined by the current collection at 0 bias, where there is still a large electrical field near the HTL-perovskite interface even in the lower EA devices, a stronger N_t dependence is expected for J_{sc}. On the other hand, V_{oc} and FF are determined by current collection at higher forward biases, where the electrical field is significantly lower with decreasing HTL energy levels. For the low EA HTL, i.e., with a marginal electrical field near the interface, the existence of even a small number of defects results in severe interfacial recombination, evidenced by large V_{oc} and FF reductions. As a combination of the three parameters, the PCE [Fig. 4(d)] of every device with lower EA HTLs suffers a dramatic decrease at low N_t, followed with a moderate further decrease with increasing N_t. For the devices with higher EA HTL, PCE only shows a very slow decrease with increasing N_t. Since attaining a defect-free ($<10^7$ cm^{-2}) interface is highly unlikely in real devices, Fig. 4 shows that increasing the HTL energy levels, rather than decreasing N_t (passivating interfacial defects), is the route toward better performance PSCs. Therefore, experimental efforts on developing HTL materials with high energy levels are highly valuable.

In conclusion, the impact of interfacial recombination and CTL electronic level positions were investigated using one-dimensional drift-diffusion device simulation in hybrid organic-inorganic metal halide perovskite solar cells. CTLs with a favorable band alignment, i.e., high electron affinity/high p-doping for hole transport layers and low electron affinity/high n-doping for electron transport layers, are shown to be beneficial for maintaining high power-conversion efficiency in the presence of recombination at the CTL-perovskite interfaces. A largely reduced minority carrier

density, due to an enhanced local electrical field, is observed near the interface when band alignment is favorable. With an unfavorable CTL energy level, device performance deteriorates significantly due to increased recombination through interfacial defects. On the other hand, only a small power-conversion efficiency decrease is observed in devices with a very high interface defect density when CTL band alignments are favorable. With the current interest to develop better CTLs for PSCs, this study provides a clear guideline for future CTL design and optimization: while interfacial defect passivation is one approach to reduce recombination at electrodes, band alignment optimization (i.e., HTLs with larger electron affinity/higher *p*-doping and ETLs with smaller electron affinity/higher *n*-doping) provides a more realistic path to suppress detrimental interfacial recombination and boost performance in PSCs.

See supplementary material for simulation parameters, simulation results for ETL, comparison between mid-gap and shallow traps, simulation results for varying N_A, field and electron density profiles for the entire devices, and non-normalized results of Fig. 4.

We would like to thank Maarten Van de Put for useful discussions on running the Sentaurus simulations. This project is supported by the University of Texas at Dallas, the Texas Photonic Center, and National Science Foundation No. DMR-1305893. J.W.P.H. acknowledges the Texas Instruments Distinguished Chair in Nanoelectronics.

[1] W. S. Yang, J. H. Noh, N. J. Jeon, Y. C. Kim, S. Ryu, J. Seo, and S. I. Seok, Science **348**, 1234 (2015).
[2] T. M. Brenner, D. A. Egger, L. Kronik, G. Hodes, and D. Cahen, Nat. Rev. Mater. **1**, 15007 (2016).
[3] Q. Lin, Nat. Photonics **9**, 106 (2014).
[4] Y. Yang, M. Yang, D. T. Moore, Y. Yan, E. M. Miller, K. Zhu, and M. C. Beard, Nat. Energy **2**, 16207 (2017).
[5] S. D. Stranks, ACS Energy Lett. **2**, 1515 (2017).
[6] H. Oga, A. Saeki, Y. Ogomi, S. Hayase, and S. Seki, J. Am. Chem. Soc. **136**, 13818 (2014).
[7] J.-P. Correa-Baena, W. Tress, K. Domanski, E. H. Anaraki, S.-H. Turren-Cruz, B. Roose, P. P. Boix, M. Gratzel, M. Saliba, A. Abate, and A. Hagfeldt, Energy Environ. Sci. **10**, 1207 (2017).
[8] I. Zarazua, G. Han, P. P. Boix, S. Mhaisalkar, F. Fabregat-Santiago, I. Mora-Seró, J. Bisquert, and G. Garcia-Belmonte, J. Phys. Chem. Lett. **7**, 5105 (2016).
[9] Y. Hou, W. Chen, D. Baran, T. Stubhan, N. A. Luechinger, B. Hartmeier, M. Richter, J. Min, S. Chen, C. O. R. Quiroz, N. Li, H. Zhang, T. Heumueller, G. J. Matt, A. Osvet, K. Forberich, Z.-G. Zhang, Y. Li, B. Winter, P. Schweizer, E. Spiecker, and C. J. Brabec, Adv. Mater. **28**, 5112 (2016).
[10] E. J. W. Crossland, N. Noel, V. Sivaram, T. Leijtens, J. A. Alexander-Webber, and H. J. Snaith, Nature **495**, 215 (2014).
[11] A. Bera, A. D. Sheikh, M. A. Haque, R. Bose, E. Alarousu, O. F. Mohammed, and T. Wu, ACS Appl. Mater. Interfaces **7**, 28404 (2015).
[12] J. Peng, Y. Wu, W. Ye, D. A. Jacobs, H. Shen, X. Fu, Y. Wan, T. Duong, N. Wu, C. Barugkin, H. T. Nguyen, D. Zhong, J. Li, T. Lu, Y. Liu, M. N. Lockrey, K. J. Weber, K. R. Catchpole, and T. P. White, Energy Environ. Sci. **10**, 1792 (2017).
[13] Y. H. Lee, J. Luo, M.-K. Son, P. Gao, K. T. Cho, J. Seo, S. M. Zakeeruddin, M. Grätzel, and M. K. Nazeeruddin, Adv. Mater. **28**, 3966 (2016).
[14] Y. Shao, Z. Xiao, C. Bi, Y. Yuan, and J. Huang, Nat. Commun. **5**, 5784 (2014).
[15] J. You, Nat. Nanotechnol. **11**, 75 (2016).
[16] C. M. Wolff, F. Zu, A. Paulke, L. P. Toro, N. Koch, and D. Neher, Adv. Mater. **29**, 1700159 (2017).
[17] R. A. Belisle, P. Jain, R. Prasanna, T. Leijtens, and M. D. McGehee, ACS Energy Lett. **1**, 556 (2016).
[18] D. B. Khadka, Y. Shirai, M. Yanagida, J. W. Ryan, and K. Miyano, J. Mater. Chem. C **5**, 8819 (2017).
[19] T. Minemoto and M. Murata, Sol. Energy Mater. Sol. Cells **133**, 8 (2015).
[20] M. Gloeckler and J. R. Sites, Thin Solid Films **480-481**, 241 (2005).
[21] H. Zhang, H. Wang, W. Chen, and A. K. Y. Jen, Adv. Mater. **29**, 1604984 (2016).
[22] W. A. Dunlap-Shohl, T. B. Daunis, X. Wang, J. Wang, B. Zhang, D. Barrera, Y. Yan, J. W. P. Hsu, and D. B. Mitzi, J. Mater. Chem. A **6**, 469 (2018).
[23] X. Yin, M. Que, Y. Xing, and W. Que, J. Mater. Chem. A **3**, 24495 (2015).
[24] A. Bera, K. Wu, A. Sheikh, E. Alarousu, O. F. Mohammed, and T. Wu, J. Phys. Chem. C **118**, 28494 (2014).
[25] Synopsys, TCAD Sentaurus: Sentaurus Device User Guide (2016; Release M-2016.12).
[26] M. Liu, M. B. Johnston, and H. J. Snaith, Nature **501**, 395 (2014).
[27] C.-G. Wu, C.-H. Chiang, Z.-L. Tseng, M. K. Nazeeruddin, A. Hagfeldt, and M. Gratzel, Energy Environ. Sci. **8**, 2725 (2015).
[28] K. Miyano, N. Tripathi, M. Yanagida, and Y. Shirai, Acc. Chem. Res. **49**, 303 (2016).
[29] J. Wang, Y.-J. Lee, and J. W. P. Hsu, J. Mater. Chem. C **4**, 3607 (2016).
[30] T. S. Sherkar, C. Momblona, L. Gil-Escrig, H. J. Bolink, and L. J. A. Koster, Adv. Energy Mater. **7**, 1602432 (2017).
[31] T. S. Sherkar, C. Momblona, L. Gil-Escrig, J. Ávila, M. Sessolo, H. J. Bolink, and L. J. A. Koster, ACS Energy Lett. **2**, 1214 (2017).
[32] H.-S. Duan, H. Zhou, Q. Chen, P. Sun, S. Luo, T.-B. Song, B. Bob, and Y. Yang, Phys. Chem. Chem. Phys. **17**, 112 (2014).